

Orthographic Star Coordinates

Dirk J. Lehmann and Holger Theisel

Abstract—Star coordinates is a popular projection technique from an n D data space to a 2D/3D visualization domain. It is defined by setting n coordinate axes in the visualization domain. Since it generally defines an affine projection, strong distortions can occur: an n D sphere can be mapped to an ellipse of arbitrary size and aspect ratio. We propose to restrict star coordinates to orthographic projections which map an n D sphere of radius r to a 2D circle of radius r . We achieve this by formulating conditions for the coordinate axes to define orthographic projections, and by running a repeated non-linear optimization in the background of every modification of the coordinate axes. This way, we define a number of orthographic interaction concepts as well as orthographic data tour sequences: a scatterplot tour, a principle component tour, and a grand tour. All concepts are illustrated and evaluated with synthetic and real data.

Index Terms—Start plot, multivariate visualization, visual analytics

1 INTRODUCTION

Projections of data points from a high-dimensional data space to a 2D (or 3D) visualization space are a common approach to visualize multi-parameter data. Such projections have to be carefully chosen. Generally, many projections are available, making the automatic or interactive choice of relevant ones a challenging task. Clearly, any projection causes a loss of information because many n D data points are mapped to the same 2D location. However, a good projection should only show properties of the data, not properties of the projection.

There are two common projection techniques used in multi-parameter data visualization: projective and affine projections. Projective projections map straight lines to straight lines and preserve the cross ratio of four collinear points [8]. Examples are RadViz [13, 14] and its modifications, as shown in [5]. Fig. 1(a) gives an illustration of a projective projection from a 3D data space to a 2D visualization plane. It is defined by placing the plane into 3D space and setting a projection center out of the plane. The two spheres depict points in data space which are mapped to ellipses in 2D. Note that a translation of the data influences location size and shape of the projections: the closer the spheres come to the projection center, the larger is their projection.

Affine projections map straight lines to straight lines and preserve the ratio of three collinear points [8]. Prominent examples are star coordinates. Fig. 1(b) shows an affine projection from 3D to 2D which is defined by setting a projection plane and a projection direction outside the plane. Also here, spheres in the data domain are mapped to ellipses.

Both projective and affine projections map points on an n D sphere onto ellipses of arbitrary aspect ratio and size. This means that the user can hardly make assumptions about the shape of an n D point cluster just from the shape of its projection. Moreover, there is no direct relation between the distance of two points in n D and in the projection: clearly, two points close to each other in the projection can be far away from each other in n D. Unfortunately, also the opposite is true: two points close to each other in n D can be far away from each other in the projection. Fig. 1(c) gives an illustration.

The main idea of this paper is to restrict the projections to a certain subset of affine projections: orthographic projections. They have the property that n D spheres of radius r are mapped to circles of the same radius r . Furthermore, the distance between two points in the projec-

tion is not larger than their distance in n D: points close to each other in n D are also close to each other in the projection. Fig. 1(d) illustrates an orthographic projection from 3D to 2D: it is an affine projection defined by placing a plane with the projection direction perpendicular to it.

Our approach assumes a metric in the n -dimensional data space, i.e., that the different dimensions are comparable to each other. This is a strong condition and not always fulfilled for all data sets. For some data sets, the dimensions have the same physical units, making the assumption of a metric space obvious. For many data sets, the dimensions do not have an obvious relation/scaling to each other. In this case, a manual normalization of the dimensions creates a metric data space. Although this normalization is sort of artificial, many well-established techniques for data analysis and visualization use the same assumption, such as scatterplot matrices and PCA. Because of this, we consider the artificial creation of a metric data space by dimension normalization a standard approach.

We extend the concept of star coordinates to orthographic projections. Star coordinates are defined by setting n coordinate axes in the 2D visualization space. We provide conditions under which a layout of coordinate axes gives an orthographic projection. Furthermore, we provide algorithms for an interactive manipulation of the coordinate axes under the constraint of remaining orthographic. Also, we describe an approach to smoothly interpolate between two orthographic projections under the same constraint. Both approaches are based on a repeated non-linear optimization in the background of every modification. For this, we discuss several numerical approaches. There are some well-established projections which are orthographic by definition: scatterplots and PCA. Hence, we incorporate them into our framework. Furthermore, we present different ways for an orthographic tour visualization: orthographic scatterplot tours (defining smooth orthographic paths between all scatterplots), orthographic PCA tours (describing smooth paths through different PCA projections), and an orthographic grand tour (by defining a space-filling curve in the space of all orthographic star plots). We also show that orthographic star plots can straightforwardly be extended to 3D star plots. We test our approach on a number of synthetic and real data sets and show the advantages compared to traditional projection techniques.

2 RELATED WORK

A number of visualization techniques exist in order to visualize high-dimensional data. Some comprehensive introduction in visualization of n D data is offered, amongst others, in [16, 12]. The focus of our paper are projection-based visualization approaches.

Affine projections: star coordinates are introduced by Kandogan et al. [18, 19]. They define a multivariate projection from n D data to a 2D visualization domain. It yields a scattered visualization similar to bivariate scatterplots, but – in contrast to them – they represent a multivariate embedding of the data, allowing a multivariate visual data

• D. J. Lehmann is with Department of Simulation and Graphics, University of Magdeburg, Germany, e-mail: dirk@isg.cs.uni-magdeburg.de
 • H. Theisel is with Department of Simulation and Graphics, University of Magdeburg, Germany, e-mail: theisel@isg.cs.uni-magdeburg.de

Manuscript received 31 March 2013; accepted 1 August 2013; posted online 13 October 2013; mailed on 4 October 2013.

For information on obtaining reprints of this article, please send e-mail to: tvcg@computer.org.

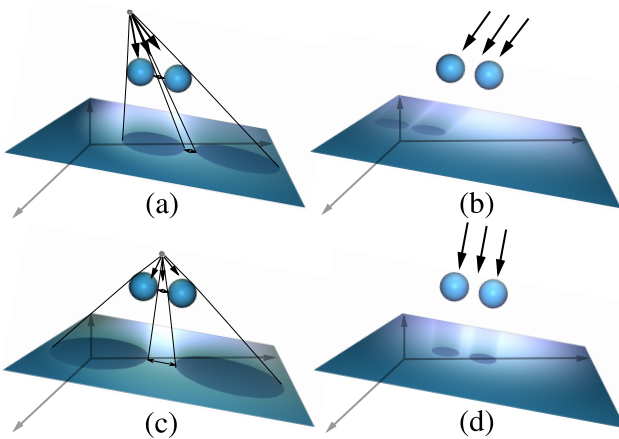


Fig. 1. (a) Projective projection from 3D data space to a 2D visualization plane. (b) Affine projection from 3D to 2D. (c) Two close points can be far away in projection. (a-c) Non-orthographic projections lead to distortions, which negatively effect the visual analysis process. (d) Orthographic projection from 3D to 2D. Ratios and sizes are preserved.

analysis. Interaction is possible by placing and moving n coordinate axes in the visualization domain. Star coordinates have been applied in [3, 21], and for the exploration of continuous attribute spaces in [22]. 3D star coordinates, e.g., from Shaik and Yeasin [26], use a 3D visualization domain.

Projective projections: RadViz, proposed by Hoffman et al. [13, 14], is another projective visualization technique similar to star coordinates but with an additional weighting factor, which is based on an underlying spring model. A variation of it is known, in order to reveal a closed free-form surface as visual representative of data, from Theisel and Kreuseler [27]. Furthermore, a normalized version of RadViz is given, and strictly investigated for their ordering properties by Daniels et al. [5] ([5] also shows that RadViz is actually a projective projection). The projection properties of RadViz (e.g., w.r.t. distortions) have been investigated by Lenka [23], DiCaro et al. [6], or Novakova et al. [24, 25]. In fact, these papers contain a number of approaches to keep the distortions induced by the projection small. We focus on preserving the property of having an orthographic projection.

Projection selection and tours: Based on such low-dimensional projections, Friedman et al. [11, 10] proposed strategies to get low-dimensional embeddings with patterns of interest for n D data. Asimov extended these approaches to the grand tour [1]: a sequence of low-dimensional projections that make a complete view of the data over time feasible. Cook et al. [4] developed some interesting variations of it. We extend this concept to an orthography-preserving version of the grand tour and further data tours.

3 APPROACH

We start with a short description of traditional 2D star coordinates. An n D point $\mathbf{m} = (m_1, \dots, m_n)^T$ is projected onto a 2D point $\mathbf{p} = (x, y)^T$ by a matrix multiplication

$$\mathbf{p} = \mathbf{A} \mathbf{m}$$

where \mathbf{A} is a $2 \times n$ matrix

$$\mathbf{A} = \begin{pmatrix} x_1 & x_2 & \dots & x_n \\ y_1 & y_2 & \dots & y_n \end{pmatrix} \quad (1)$$

which completely defines the projection. The entries of \mathbf{A} have a nice interpretation: defining $\mathbf{p}_i = (x_i, y_i)^T$ for $i = 1, \dots, n$, the vectors $(\mathbf{p}_i - \mathbf{0})$ describe the projections of the n D coordinate axes into the 2D domain ($\mathbf{0}$ is the 2D origin). The axes $(\mathbf{p}_i - \mathbf{0})$ are either placed in certain setups (such as a radial alignment), or they can interactively be modified by moving the points \mathbf{p}_i .

In order to find conditions of \mathbf{A} for defining orthographic projections, we introduce two n D vectors consisting of the x - and y -coordinates of all \mathbf{p}_i , respectively:

$$\mathbf{x} = (x_1, \dots, x_n)^T, \mathbf{y} = (y_1, \dots, y_n)^T.$$

An orthographic projection can be described as concatenation of a rotation in n D and a subsequent projection onto the first two coordinate axes, i.e., a “cutting-off” of the 3-rd to n -th coordinate:

$$\mathbf{A} = \begin{pmatrix} 1 & 0 & 0 & \dots & 0 \\ 0 & 1 & 0 & \dots & 0 \end{pmatrix} \mathbf{R} \quad (2)$$

where \mathbf{R} is an $n \times n$ rotation matrix. This means that the columns of \mathbf{R} build an orthonormal system: all column vectors have unit length and are perpendicular to each other. Note that in (2) large parts of \mathbf{R} do not have any influence on \mathbf{A} . In fact, only the first two lines of \mathbf{R} are relevant. We use a basic property of rotation matrices: if \mathbf{R} is a rotation matrix, then its transposed \mathbf{R}^T is a rotation matrix as well. Since (1) and (2) give

$$\mathbf{R}^T = (\mathbf{x}, \mathbf{y}, \dots),$$

the condition for \mathbf{A} being orthographic is

$$\|\mathbf{x}\|^2 = 1, \quad \|\mathbf{y}\|^2 = 1, \quad \langle \mathbf{x}, \mathbf{y} \rangle = 0, \quad (3)$$

where $\langle *, * \rangle$ is the scalar product. From this we define an orthographic energy which quantizes how far away a matrix \mathbf{A} is from being orthographic:

$$e(\mathbf{A}) = (\|\mathbf{x}\|^2 - 1)^2 + (\|\mathbf{y}\|^2 - 1)^2 + \langle \mathbf{x}, \mathbf{y} \rangle^2. \quad (4)$$

Note that $e(\mathbf{A}) \geq 0$, and $e(\mathbf{A}) = 0$ iff \mathbf{A} is orthographic. We subsequently use the symbol \mathbf{A}^π to address such an orthographic projection, i.e., $[\mathbf{A} = \mathbf{A}^\pi] \Leftrightarrow [e(\mathbf{A}) = 0]$. The larger the energy e , the more distorted an n D shape is under projection. Figure 2 illustrates this. On

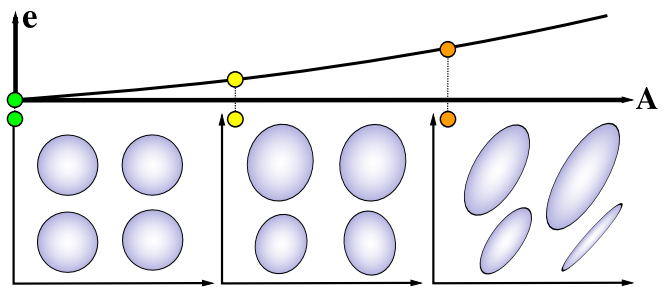


Fig. 2. Schematic illustration of Orthographic Energy: (top) Energy graph e depending on different projections A . (bottom) Projection results of n D spheres related to certain energy levels. The larger the energy, the stronger the distortion gets.

top, a potential energy graph e is plotted. At the bottom, three samples (green, yellow, orange) are given, representing different axis configurations. \mathbf{A}_{green} has a minimum energy $e(\mathbf{A}_{green}) = 0$ and shows no projection-based distortions. Consequently, this projection is orthographic. In contrast, larger energy yields stronger distortions. Please compare \mathbf{A}_{yellow} and \mathbf{A}_{orange} . Both radii and size are unfavorably distorted under projection. For searching for \mathbf{A}^π , minimizing $e(\mathbf{A})$ is required. For that, non-linear optimizers are necessary, since $e(\mathbf{A})$ is of polynomial degree 4 in the components of \mathbf{A} .

3.1 Revealing 2D Orthographic Star Coordinates

An arbitrary start configuration of axes \mathbf{A} does not yield orthographic star coordinates (OSC) in the vast majority of cases, i.e., a random configuration equates to non-orthographic star coordinates (NSC), which do not fulfill the conditions of Eq. (3), i.e., $e(\mathbf{A}) > 0$. The question arises how an OSC can be efficiently revealed from an initial NSC. Subsequently, two techniques are presented.

3.1.1 Revealing 2D OSC by Reconditioning

The first approach is a geometrical approach, based on the Gram-Schmidt process [20], in order to reconstruct the necessary conditions geometrically. For this, the conditions of Eq. (3) are restored step by step in order to transform a configuration of axes $\mathbf{A} = (\mathbf{x}, \mathbf{y})^T$, which gives an NSC, into an axes configuration \mathbf{A}^π , which gives an OSC.

First, the condition that \mathbf{x} is orthogonal to a certain vector \mathbf{y}^π , i.e. $\langle \mathbf{x}, \mathbf{y}^\pi \rangle = 0$, is restored with

$$\mathbf{y}^\pi = \mathbf{y} - \frac{\mathbf{x}}{\|\mathbf{x}\|} \cdot \frac{\mathbf{x}}{\|\mathbf{x}\|} \leftrightarrow \langle \mathbf{x}, \mathbf{y}^\pi \rangle = 0.$$

Then, the condition of having an Euclidean norm of one can be easily reconstructed by normalizing the axis with

$$\mathbf{x}_n = \frac{\mathbf{x}}{\|\mathbf{x}\|} \quad \text{and} \quad \mathbf{y}_n^\pi = \frac{\mathbf{y}^\pi}{\|\mathbf{y}^\pi\|} \leftrightarrow \|\mathbf{x}_n\| = \|\mathbf{y}_n^\pi\| = 1.$$

Please note that vectors \mathbf{x}_n , \mathbf{y}^π , and \mathbf{y}_n^π lie in the same plane that is spanned by \mathbf{x} and \mathbf{y} in n D. Finally, the transformation from \mathbf{A} to \mathbf{A}^π is given by

$$\mathbf{A} \rightarrow \mathbf{A}^\pi := (\mathbf{x}_n, \mathbf{y}_n^\pi)^T.$$

This geometry-based reconditioning does not need any parameters and can be done with low costs of $O(n)$.

3.1.2 Revealing 2D OSC by Energy Minimization

The above-mentioned orthographic energy measure $e(\mathbf{A})$ of Eq. (4) gives us an alternative approach to transform an initial \mathbf{A} into \mathbf{A}^π by performing an iterative gradient descent-based energy minimization: $e(\mathbf{A}) \rightarrow \min$. Let ∇e be the gradient of energy $e(\mathbf{A})$ given as the following matrix nomenclature

$$\nabla e = \begin{pmatrix} e_{x_1} & e_{x_2} & \dots & e_{x_n} \\ e_{y_1} & e_{y_2} & \dots & e_{y_n} \end{pmatrix},$$

with its partial derivatives $e_{x_j} = \partial e / \partial x_j$ and $e_{y_j} = \partial e / \partial y_j$ given by

$$\begin{aligned} e_{x_j} &= 4 \cdot x_j \cdot (\|\mathbf{x}\|^2 - 1) + 2 \cdot y_j \cdot \langle \mathbf{x}, \mathbf{y} \rangle \quad \text{and} \\ e_{y_j} &= 4 \cdot y_j \cdot (\|\mathbf{y}\|^2 - 1) + 2 \cdot x_j \cdot \langle \mathbf{x}, \mathbf{y} \rangle. \end{aligned} \quad (5)$$

Then, successor \mathbf{A}_{i+1} that minimizes energy e is reachable via an Euler step based on \mathbf{A}_i as:

$$\mathbf{A}_{i+1} \rightarrow -\mu \cdot \nabla e(\mathbf{A}_i) + \mathbf{A}_i,$$

with μ being the step size. Please note that gradient ∇e points in direction of the steepest ascent of e . Therefore, the descent has to go in negative direction of the gradient in order to minimize the energy. In the limit $i \rightarrow \infty$ the series \mathbf{A}_{i+1} converges against the orthographic matrix \mathbf{A}^π (i.e., $\mathbf{A} \rightarrow \mathbf{A}^\pi := \mathbf{A}_\infty = \mathbf{A}^\pi$ with $\mathbf{A}_0 = \mathbf{A}$). In practice, the descent is stopped either after an iteration number of $i = s$ or if e falls below a certain threshold. Thus, the energy minimization requires two input parameters (the iteration number s and the step size μ) and it requires the costs of $O(n \cdot s)$.

Fig. 3 schematically illustrates the idea of the reconditioning (top-left) and the energy minimization (top-right) in order to reveal a configuration of axes \mathbf{A}^π that guarantees an OSC-based on a non-orthographic configuration \mathbf{A} . Additionally, Fig. 3 (bottom) illustrates results of the approach based on a 5D random non-orthographic configuration of axes (left), for the reconditioning (middle) and the energy minimization by gradient descent (right) in comparison. A detailed evaluation of these techniques is given in Section 4.

3.2 Initial 2D Orthographic Star Coordinates

In most cases, the user requires an instant initial 2D OSC directly after a certain high-dimensional data set is loaded, and without using the prior described detour via an NSC. Thus, in this section, two approaches are given in order to visually initiate such data as a 2D OSC instantly.

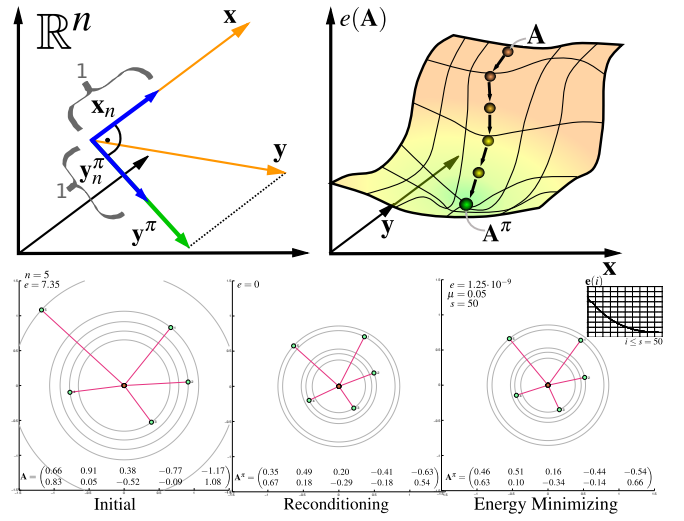


Fig. 3. Revealing 2D Orthographic Star Coordinates: (top-left) Illustration for the concept of reconditioning and (top-right) energy minimization. (bottom-left) By applying both concepts to the same random axes configuration, both the reconditioning (bottom-middle) and the energy minimization (bottom-right) provide a better axes configuration. Please note that energy minimization needs to be parameterized nonetheless.

3.2.1 Initial 2D OSC by Radial Standard Configuration

A modest approach to reveal an initial \mathbf{A}^π for an n -dimensional data set is given by assigning the anchor points of the axis $\mathbf{A}^\pi = (\mathbf{x}, \mathbf{y})^T$ regularly along the periphery of a circle with radius r , given by

$$(x_i, y_i)^T = r \cdot (\sin(i \cdot \alpha), \cos(i \cdot \alpha))^T; i = 0, \dots, n-1.$$

By choosing $\alpha = 2\pi/n$ and $r = \sqrt{2}/n$, it can be guaranteed to obtain an orthographic projection. Thus, the radial standard configuration requires no input parameters, and additionally it runs quickly in $O(n)$. Please note that both r and α shrink with the dimension number n and thus $r = 0$ and $\alpha = 0$ in the limit $n \rightarrow \infty$. Figure 4 illustrates this for standard configurations of the dimension numbers $n = 3, \dots, 8$. This means the approach is sensitive for the number of dimensions n , but it is not yet sensitive for semantic information within the data. This drawback is addressed in the next section.

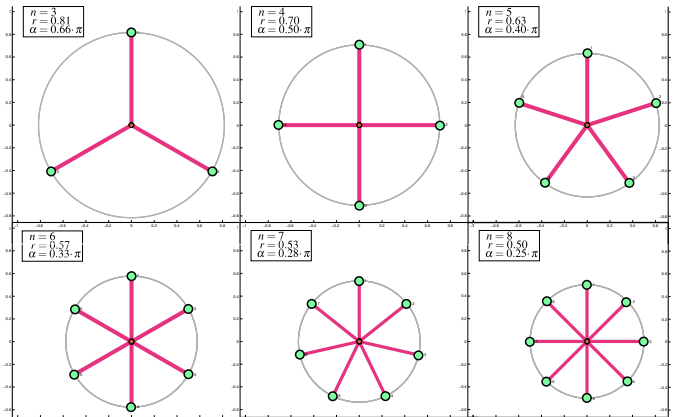


Fig. 4. Radial Standard Configuration for 2D Orthographic Star Coordinates: from top-left to right-bottom, the dimension number n increases from 3 to 8. Radius r and angle α shrink with the dimension number n .

3.2.2 Initial 2D OSC by PCA Configuration

On the one hand, the previous approach supports the user by presenting an OSC. On the other hand, such an initial configuration is equal

if the number of dimensions is equal. Obviously, it would rather be desired to have initial 2D star coordinates with both the orthographic property and a semantic relation to the data. Fortunately, this can be realized straightforwardly by applying a principal component analysis (PCA) on the data.

The well-known PCA is – briefly described – an $n \times n$ matrix $\mathbf{E} = (\mathbf{e}_1, \mathbf{e}_2, \dots, \mathbf{e}_n)$ of the (column-wise) eigenvectors $\mathbf{e}_j = \mathbf{e}_{1 \times n}(\lambda_j)$ to the spectrum (or sorted eigenvalues) $\lambda_j; j = 1, \dots, n$ of the covariance matrix $\mathbf{C}(\mathbf{M}^T \cdot \mathbf{M})$ from high-dimensional data $m \in \mathbf{M}$. For details, please see [15, 17, 7, 9]. The PCA defines a rotation from the n -dimensional canonical basis of Euclidean data space onto an orthonormal basis – given by the eigenvectors \mathbf{e}_j – so that variance and amount of information, respectively is maximized in those directions which are related to the largest spectrum values λ_j . Thus, the vectors of the basis are mutually orthogonal with unit length, i.e., they fulfill Eq. (3) and therefore reveal an orthographic projection. Hence, an initial configuration is given by

$$\mathbf{A}^\pi(i, j) := (\mathbf{e}_i, \mathbf{e}_j)^T. \quad (6)$$

This PCA-based configuration requires pair i, j as initial dimension of interest as input parameters by consuming costs of $O(n \cdot m)$ for $m > n$, else $O(n^2)$. It is advisable to choose $i, j; i \neq j$ so that they are related to large eigenvalues in order to maximize the relevance of the initial OSC w.r.t. the visualized information. However, the outcome is an OSC that is both sensitive to the number of dimensions as well as to semantic properties of the data. This gives a better starting point for a visual exploration than the previous approach. For illustration, Fig. 5 provides PCA configurations for the *Iris* data set with $n = 4$ dimensions and for the *Wine* data set with $n = 13$ dimensions. See Section 4 and [2] for data details. It can be seen that the initial orthographic configuration is aligned to semantics of the data.

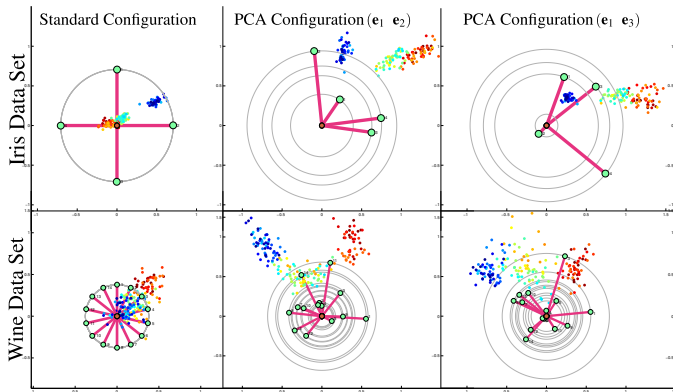


Fig. 5. (left) Radial Standard Configuration and (middle-right) PCA configuration to the largest eigenvalues for (top) the Iris data set with $n = 4$ dimensions and (bottom) the Wine data set with $n = 13$ dimensions. Note that class information are not supported. Each record is individually colorized to enable a record-based comparison. It can be seen that solely the PCA configuration is sensitive to semantics of the data.

3.3 Interaction with 2D Orthographic Star Coordinates

Until here, approaches to generate 2D OSCs of n -dimensional data, either from an NOC or directly from the data, have been defined. They are the initial step for a visual exploration. The next step is to define convenient 2D OSC interaction approaches w.r.t. the coordinate axes. Assuming that an orthographic projection $\mathbf{A}^\pi = (\mathbf{p}_1 \mathbf{p}_2 \dots \mathbf{p}_n)$ is already available: by interactively moving an axis \mathbf{p}_1 to its new position $\mathbf{p}_1^b = \mathbf{p}_1 + \mathbf{s}_1$, the remaining axes $\mathbf{p}_i; i = 2, \dots, n$ need to be automatically shifted – with shift vectors \mathbf{s}_i – to a new position $\mathbf{p}_i^b; i = 2, \dots, n$ that guarantees to preserve an orthographic projection. The resulting orthographic projection, after the interaction is done, is symbolized by

$\mathbf{A}^\pi_b = (\mathbf{p}_1^b \mathbf{p}_2^b \dots \mathbf{p}_n^b)$. Consequently, orthography-preserving interaction is given by transforming the axis configuration \mathbf{A}^π to \mathbf{A}^π_b and it equates to the task of carefully choosing shift vectors $\mathbf{s}_i; i = 2, \dots, n$. We restrict ourselves to discuss interactions only for the axis \mathbf{p}_1 . Fig. 6 illustrates this as well as the subsequently used mathematically notations with the aid of the example for the case $n = 5$. Different interaction axes can be simply utilized by adopting the used indexation within this section as needed. The issue ends up in solving a non-linear optimization for the remaining axis configuration.

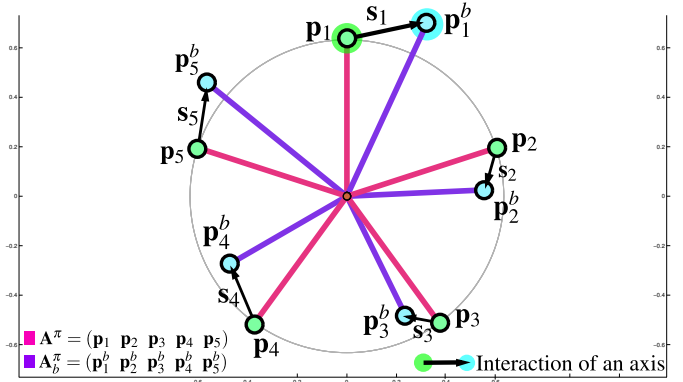


Fig. 6. Orthography-preserving interaction with the axes of Orthographic Star Coordinates: The initial axes configurations before the interaction are given in red and are still described with the symbol \mathbf{A}^π . Interaction means to move the endpoint of axis $\mathbf{p}_1 \in \mathbf{A}^\pi$ to its new position \mathbf{p}_1^b , described by the shift vector \mathbf{s}_1 . Then, the remaining axes $\mathbf{p}_i; i = 2, \dots, n$ have to be automatically shifted with shift vectors \mathbf{s}_i in such a way that an orthographic projection is still guaranteed. These shifted axes – named as $\mathbf{p}_i^b; i = 2, \dots, n$ – form the axes configuration after interaction, illustrated in blue and with the aid of symbol \mathbf{A}^π_b .

3.3.1 Analytical Orthography-Preserving Axis Interaction

We assume that the user interactively moves the axis \mathbf{p}_1 to its new position \mathbf{p}_1^b with the aid of a shift vector \mathbf{s}_1 , as illustrated in Fig. 6. The positions of remaining axes $\mathbf{p}_i; i = 2, \dots, n$ need to be adjusted to preserve the orthographic projection, which is a non-linear optimization issue, as mentioned above. However, as illustrated in the Appendix, this non-linear issue can be transformed (for each interaction step) into a certain linear system. Solving this system for a certain configuration of axes and shifts results in the new axis positions. Thus, for each interaction step no input parameters are required, but there are costs between $O(n^2)$ and $O(n^3)$ (depending on the decomposition approach) due to a QR decomposition of the linear system, required for each interaction step.

3.3.2 On the Fly Orthography-Preserving Axis Interaction

A small shift \mathbf{s}_1 of an OSC \mathbf{A}^π yields an NSC \mathbf{A} . Thus, by adjusting the techniques of Section 3.1, further strategies can be derived to conduct an orthography-preserving interaction. First, the remaining and yet unknown axes $\mathbf{p}_i^b = (x_i^b \ y_i^b)^T$ can be revealed with the proposed iterative energy minimization approach by a slight modification of it: (i) the approach is initialized with $\mathbf{A}_0 = (\mathbf{p}_1^b \ \mathbf{p}_2^b \dots \mathbf{p}_n^b)$, and (ii) the partial derivatives (cf. Eq. (5)) for $e_{x_1^b}$ and $e_{y_1^b}$ are set to zero: $e_{x_1^b} = 0, e_{y_1^b} = 0$. Then, the energy minimization yields the orthographic projection \mathbf{A}^π_b . This energy minimization still requires the same input parameters and has the same costs. Please note that for a small variation of \mathbf{A}^π by \mathbf{s}_1 the orthographic energy only marginally increases. Thus, it can be expected that already four or five steps of the descent converges in a good result, i.e., this approach is rather quick. The second possibility to reveal the unknown axes is to apply a reconditioning to $\mathbf{A}_0 = (\mathbf{p}_1^b \ \mathbf{p}_2^b \dots \mathbf{p}_n^b)$. Please note that reconditioning shares all required shifts – more or less uniformly – over all available axis components in order to reveal an OSC. Thus, also the interactively placed axis \mathbf{p}_1^b

will be mapped onto a new axis \mathbf{p}_1^{b*} by the reconditioning. The error d for this is given by the Euclidean norm $d = \|\mathbf{p}_1^{b*} - \mathbf{p}_1^b\|^2$. Since the orthographic energy only marginally increases during the interaction, it can be expected that d is generally negligible. For this approach, no parameters are required, and the linear costs of n offers the fastest of the mentioned approaches.

Fig. 7 presents an $n = 5$ D example for both “on the fly” orthography-preserving approaches in order to interact with an OSC. In conclusion, both approaches are faster than the analytical approach, but need to be parameterized or might produce a small error w.r.t. the goal axis \mathbf{p}_1^b .

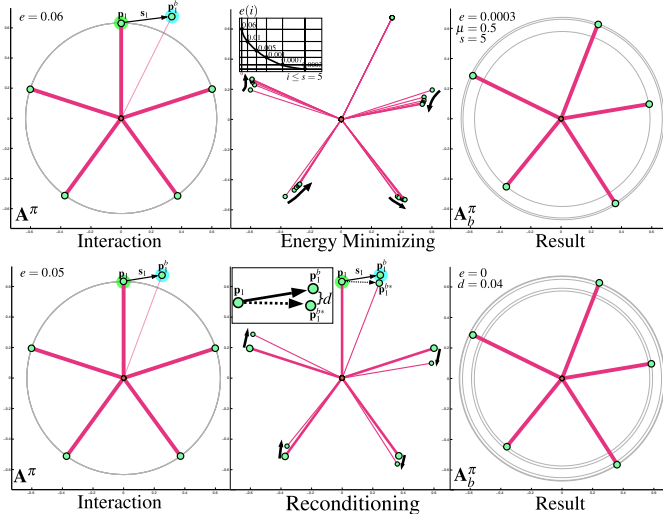


Fig. 7. On the fly orthography-preserving interaction: (top) Energy Minimization for interaction. The initial Orthographic Star Coordinates on the left are used for interacting with axis \mathbf{p}_1 , illustrated by the black arrow. In the middle, the five intermediate steps of the axes during the descent with step size $\mu = 0.5$ can be seen. On the left, the new orthography-preserving axis configuration can be seen after the interaction. Only a small error occurred during this approach given by energy $e = 0.0003$. (bottom) Reconditioning for interaction. The initial Orthographic Star Coordinates on the left are used for interacting with axis \mathbf{p}_1 , illustrated by the black arrow. In the middle, the shift for all further axes can be seen during the reconditioning. On the left, the new orthography-preserving axis configuration can be seen after the interaction. No error occurred during this approach given by energy $e = 0$, but a small offset $d = 0.04$ between the desired axis position \mathbf{p}_1^b and its real final position \mathbf{p}_1^{b*} is the cost for this energy optimum.

3.4 Conditional Interaction with 2D Orthographic Star Coordinates

In certain situations, it might be desired to satisfy conditions/restrictions for adjusting the axes $\mathbf{p}_i, i > 1$, while an interaction is conducted. In other words: it might be useful to restrict the degrees of freedom for the axes. Fig. 8 illustrates the three restrictions of interest:

1. **Fixed:** Forbid any movement, i.e., $\mathbf{p}_i = \mathbf{p}_i^b$.
2. **Radial Movement:** Allow movement solely tangential to the periphery of \mathbf{p}_i , i.e., $\|\mathbf{p}_i\| = \|\mathbf{p}_i^b\|$.
3. **Directional Movement:** Allow movement solely in the direction of \mathbf{p}_i , i.e., $\mathbf{p}_i = c \cdot \mathbf{p}_i^b$.

We assume that each axis $\mathbf{p}_i, i > 1$ is assigned with at most one of these restrictions, which means the conditions are mutually disjunct. To realize the conditions, the above-mentioned “on the fly” orthography-preserving approaches will be adopted.

First, the energy minimization can be adopted: For each fixed axis \mathbf{p}_i , the related partial derivative of Eq. (5) is set to zero: $e_{x_i^b} = 0, e_{y_i^b} =$

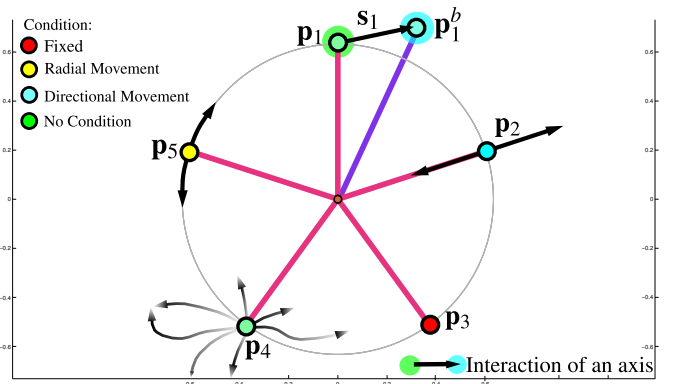


Fig. 8. Conditional orthography-preserving interaction with the axes of Orthographic Star Coordinates: To further improve the interaction options, the degree of freedom of the axes can be restricted by certain conditions w.r.t. their allowed movement. Conditions that make sense are: Fixed - the axis is fixed and not allowed to move (red), Radial Movement - the axis is allowed to move only along to the periphery (yellow), Directional Movement - the axis is allowed to move along its orientation (light blue), No Condition - the axis is allowed to move freely (green).

0. In order to include both the radial movement and the directional movement restriction, two further energy terms are added to the energy of Eq. (4): the radial movement energy term with

$$e_{radial} = \left(\sum_{i=1}^{\#radial} (\|\mathbf{p}_i^b\| - \|\mathbf{p}_i\|)^2 \right)^2,$$

and the directional movement term with

$$e_{dir} = \left(\sum_{j=1}^{\#dir} \left(\frac{\mathbf{p}_j^b \cdot \mathbf{p}_j}{\|\mathbf{p}_j^b\| \cdot \|\mathbf{p}_j\|} - 1 \right)^2 \right)^2.$$

Since the restrictions and the orthography property can be mutually conflicting, a weighting parameter $g \in \{0, 1\}$ steers the influence of the properties, which yield the adopted energy function e_c for the gradient descent w.r.t Sec. 3.1.2 with:

$$e_c = (1-g) \cdot e + g \cdot (e_{radial} + e_{dir}).$$

Now, the approach requires three parameters, namely one more with g , but still runs with costs of $O(n \cdot s)$

Second, the reconditioning technique can be transformed into another iterative gradient descent approach, for which the conditions are held, while simultaneously an iterative and ongoing reconditioning is running: Let Ω_r be a reconditioning operation applied to matrix \mathbf{A} : $\mathbf{A}^\pi = \Omega_r(\mathbf{A})$. As a reminder, please be aware that Ω_r reveals an OSC \mathbf{A}^π by reconstructing required properties within this plane that is spanned by its components \mathbf{x} and \mathbf{y} . Further, let Φ be an operation that replaces column vectors \mathbf{p}_i^* of matrix \mathbf{A}_* based on column vectors \mathbf{p}_i of matrix \mathbf{A} that are assigned with a condition as follows: $\Phi(\mathbf{A}_*, \mathbf{A}) :=$

$$\begin{aligned} (\mathbf{p}_i \text{ is fixed}) &\leftrightarrow (\mathbf{p}_i^* = \mathbf{p}_i) \\ (\mathbf{p}_i \text{ with radial movement}) &\leftrightarrow \left(\mathbf{p}_i^* = \frac{\mathbf{p}_i^b \cdot \mathbf{p}_i}{\|\mathbf{p}_i^b\|} \mathbf{p}_i \right) \\ (\mathbf{p}_i \text{ with directional movement}) &\leftrightarrow \left(\mathbf{p}_i^* = \mathbf{p}_i \cdot \frac{\langle \mathbf{p}_i^b \cdot \mathbf{p}_i \rangle}{\langle \mathbf{p}_i^b \cdot \mathbf{p}_i^* \rangle} \mathbf{p}_i^* \right). \end{aligned}$$

A simple scalar measure that describes the difference between an arbitrary axis configuration \mathbf{A}_* and an axis configuration $\Phi(\mathbf{A}_*, \mathbf{A})$ with realized conditions is given by the (component-wise) difference between \mathbf{A}_* and $\Phi(\mathbf{A}_*, \mathbf{A})$. This measure equates to the Frobenius norm $f = \|\Phi(\mathbf{A}_*, \mathbf{A}) - \mathbf{A}_*\|_F$. By choosing $\mathbf{A}_0 = \Omega_r(\mathbf{A})$, the successor \mathbf{A}_{i+1} that minimizes f and that is orthography-preserving is given by

$$\mathbf{A}_{i+1} \rightarrow \Omega_r(\Phi(\mathbf{A}_i, \mathbf{A})).$$

Please note that this series \mathbf{A}_{i+1} equates to an n D rotation of the hyperplane that is spanned by \mathbf{x}_{i+1} and \mathbf{y}_{i+1} in this direction where f is minimized. The series \mathbf{A}_{i+1} preserves the orthographic property for any $i \in \mathbb{N}$, and it converges in the limit $i \rightarrow \infty$ against this n D plane (w.r.t. \mathbf{x}_{i+1} and \mathbf{y}_{i+1}) that minimizes the distance to the conditions in least-square sense. Therefore, three advantages in comparison to energy minimization follow: (i) the orthography property is preserved in all circumstances, (ii) the conditions are realized until they are in conflict with the orthography property, and (iii) solely one parameter is required (in contrast to three parameters μ, g , and s): the iteration is stopped after an iteration number of $i = s$. Thus, the interaction with conditions requires costs of $O(n \cdot s)$ for this adjusted reconditioning technique. Figure 9 illustrates the mentioned concepts for a conditional interaction with OCSs.

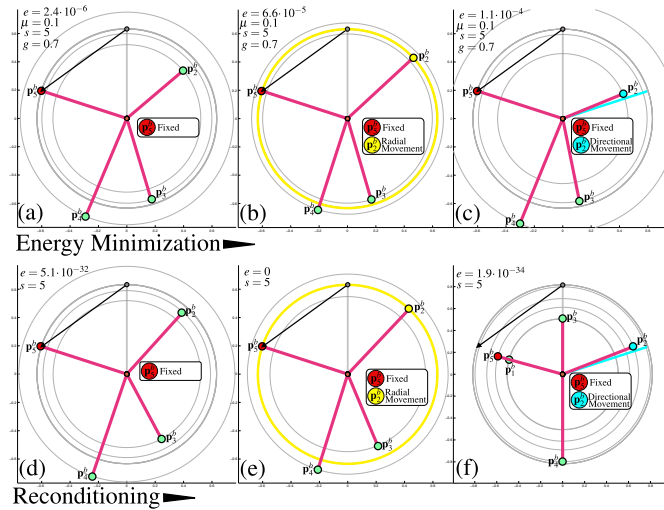


Fig. 9. On the fly conditional orthography-preserving interaction for case $n = 5$: The initial axes configuration – before the interaction – equates to the Radial Standard Configuration and is therefore not shown here. For each example, the axis \mathbf{p}_5^b is slowly moved to the axis \mathbf{p}_5^b along the pathway emphasized by the black arrow. Note that thus the axis \mathbf{p}_5^b is finally hidden and covered by the axis \mathbf{p}_5^b . All sub-images show the final results after the interaction based on different conditions that are applied to the axis. (top) Results for the energy minimization approach: (a) The axis \mathbf{p}_5^b has a fixed condition. During the interaction this axis did not move. (b) The axis \mathbf{p}_5^b still has a fixed condition. In addition, the axis \mathbf{p}_5^b has a radial movement condition, i.e., it is only allowed to move along the yellow periphery. It can be seen that this axis does not leave this periphery during interaction. (c) The axis \mathbf{p}_5^b still has a fixed condition. In addition, the axis \mathbf{p}_5^b has a directional movement condition, i.e., it is only allowed to move along the light blue line. It can be seen that this axis lies almost on that line after interaction. A small error occurred due to the large step size of $\mu = 0.1$. However, in comparison to (a-b) the direction of this axis is preserved in (c) best by far. (bottom) Results for the reconditioning approach: the conditions of the axis and the interaction results from (d-f) equate to the case for energy minimization (a-c). For the reconditioning approach it can be seen that the orthography preserving works better. The cost for that is that the conditions of the axis cannot be preserved perfectly in any cases, e.g., in (f).

3.5 Morphing between Orthographic Star Coordinates

Yet, initialization techniques as well as interaction techniques (unconditioned and conditioned) have already been defined. Now, we discuss orthography-preserving morphing approaches between two different OCSs \mathbf{A}_{start}^π and \mathbf{A}_{end}^π of same dimensionality. Fig. 10(a) shows the space of possible axis configurations. It can be seen that orthographic projections as \mathbf{A}_{start}^π and \mathbf{A}_{end}^π are connected with each other via a set of orthography-preserving axis configurations, e.g., along a certain path within this space. The trivial approach for a morphing is given by

a linear blending over time $t \in [0, 1]$ with

$$\mathbf{A}(t) = (1-t) \cdot \mathbf{A}_{start}^\pi + t \cdot \mathbf{A}_{end}^\pi,$$

but it cannot be guaranteed that the intermediate steps $\mathbf{A}(t)$ are orthographic, as seen in Fig. 10(a). Thus, at each time step t of the blending either an additional energy minimization Ω_e or a reconditioning Ω_r is required to be applied to $\mathbf{A}(t)$:

$$\mathbf{A}^\pi(t) = \rho((1-t) \cdot \mathbf{A}_{start}^\pi + t \cdot \mathbf{A}_{end}^\pi), \quad (7)$$

with $\rho \in \{\Omega_r, \Omega_e\}$; which is denoted as *Blending Energy Minimization* or *Blending Reconditioning*. As Fig. 10(b) illustrates, this treatment is orthography-preserving, but it might lead to a non-uniform sampling along the orthographic projections (orange path) that connects \mathbf{A}_{start}^π with \mathbf{A}_{end}^π . By adjusting Eq. (7), this drawback can be improved by introducing a stepwise approach: let $t_d = 1, \dots, k$ be discrete time steps and k the total number of time step samples in order to reach \mathbf{A}_{end}^π starting from \mathbf{A}_{start}^π . Then, the series $\mathbf{A}_{t_{d+1}}^\pi$ reveals a better sampling, illustrated in Fig. 10(c):

$$\mathbf{A}_{t_{d+1}}^\pi \rightarrow \rho((1 - \frac{t_d}{k}) \cdot \mathbf{A}_{t_d}^\pi + (\frac{t_d}{k}) \cdot \mathbf{A}_{end}^\pi),$$

with $\mathbf{A}_0^\pi = \mathbf{A}_{start}$ and $t_d \in \mathbb{N} \leq k$. Since the distance to an orthographic projection, described by energy e , is lower for each intermediate step $\mathbf{A}_{t_d}^\pi$ in comparison to the previous approach, the required iteration number s for energy minimization in order to reach an orthographic projection is lower than before, i.e., the approach is faster than before.

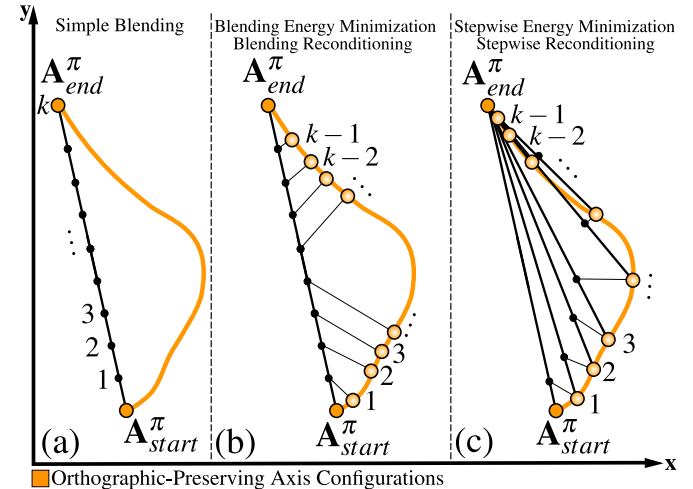


Fig. 10. Schematic Illustration for morphing between two orthographic axis configurations \mathbf{A}_{start}^π and \mathbf{A}_{end}^π : The space of all possible axis configurations is given by x and y . \mathbf{A}_{start}^π and \mathbf{A}_{end}^π are two orthographic representatives in that space, and they are connected with each other via an orange path. Only that path consists of further orthographic configurations, i.e., $e = 0$, and it should be ideally run through during the morphing from \mathbf{A}_{start}^π to \mathbf{A}_{end}^π . (a) A simple linear blending between \mathbf{A}_{start}^π and \mathbf{A}_{end}^π delivers the intermediate axis configurations on the black line. These intermediate axes equate to non-orthographic projections in general. (b) By applying a reconditioning/energy minimization during the simple linear blending, the orthographic property is preserved, i.e., the intermediate steps lie on the orange path. However, non-uniform distributions of samples on the orange path occur. (c) The stepwise approach improves the distribution of intermediate steps.

Fig. 11 illustrates examples for all introduced morphing approaches. The maximum orthographic energy is maximal for a simple blending, smaller for an energy minimization approach (with $\mu = 0.1, s = 5$), and smallest for the reconditioning approach.

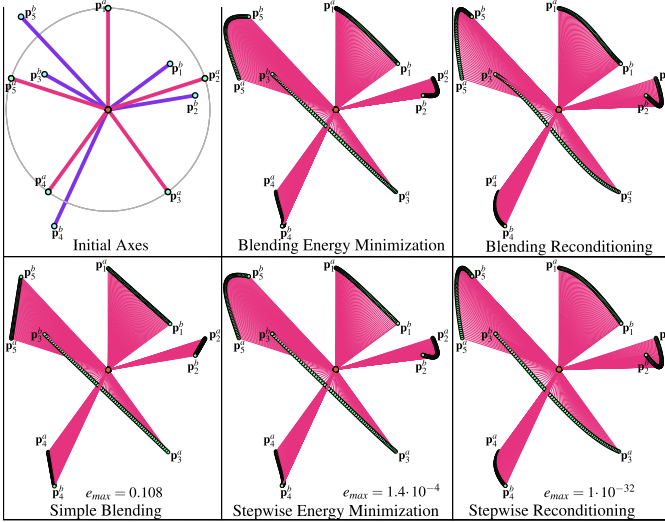


Fig. 11. Examples for the morphing approaches: (top-left) Initial configuration for the orthographic axis configurations \mathbf{A}_{start}^π (red) and \mathbf{A}_{end}^π (blue). (top-middle to bottom-right) Morphing approaches in comparison: the intermediate axes are illustrated overlaid for $k = 70$ steps.

3.6 Data Tours

In order to support the exploration of large nD data, our OSC morphing approaches allow to define several data tour strategies. The main idea is to sample certain axis configurations and to apply a morphing between each sample pair in order to reveal a smooth tour. For this, we assume a method $Morphing(\mathbf{A}_{start}, \mathbf{A}_{end}, k)$, which applies a morphing between the start projection \mathbf{A}_{start} and the end projection \mathbf{A}_{end} in k steps w.r.t. any above introduced morphing approach.

3.6.1 Scatterplot Tour

A bivariate orthographic version of star coordinates projection is a scatterplot. A scatterplot is a bivariate visualization technique that visualizes two dimensions of the nD data via a $2 \times n$ matrix $\mathbf{A}_{i,j}; i \neq j$ and all of its column permutations, given by a zero matrix, except for index i and j ; there, it applies $\mathbf{p}_i = (1, 0)^T$ and $\mathbf{p}_j = (0, 1)^T$, e.g., $\mathbf{A}_{1,2}$ and $\mathbf{A}_{4,3}$ are given by:

$$\mathbf{A}_{1,2} = \begin{pmatrix} 1 & 0 & 0 & 0 & 0 & \dots \\ 0 & 1 & 0 & 0 & 0 & \dots \end{pmatrix}, \quad \mathbf{A}_{4,3} = \begin{pmatrix} 0 & 0 & 0 & 1 & 0 & \dots \\ 0 & 0 & 1 & 0 & 0 & \dots \end{pmatrix}.$$

By avoiding repetitions of configurations, there are $\frac{n(n-1)}{2}$ permutations and different scatterplots available. The orthography-preserving tour that visits all scatterplots of an nD data is given by Alg. 1.

Algorithm 1 Scatterplot Tour(\mathbf{A}, k)

```

 $\mathbf{A}_{start} = \mathbf{A}$ 
for  $i=1$  to  $n$  do
  for  $j=i+1$  to  $n$  do
     $\mathbf{A}_{end} = \mathbf{A}_{i,j}$ 
     $Morphing(\mathbf{A}_{start}, \mathbf{A}_{end}, k)$ 
     $\mathbf{A}_{start} = \mathbf{A}_{i,j}$ 
  end for
end for

```

3.6.2 PCA Tour

By following this scheme, an orthographic-preserving PCA-based tour can be defined. Sec. 3.2.2 already introduced the PCA matrix \mathbf{E} with its column vectors $\mathbf{e}_i; i = 1, \dots, n$. The PCA tour that completely visits the PCA basis vector configurations, sorted by size of the related eigenvalues, is given by Alg. 2.

Algorithm 2 PCA Tour(\mathbf{A}, k)

```

 $\mathbf{A}_{start} = \mathbf{A}$ 
for  $j=2$  to  $n$  do
  for  $i=1$  to  $j$  do
     $\mathbf{A}_{end} = (\mathbf{e}_i \ \mathbf{e}_j)^T$ 
     $Morphing(\mathbf{A}_{start}, \mathbf{A}_{end}, k)$ 
     $\mathbf{A}_{start} = (\mathbf{e}_i \ \mathbf{e}_j)^T$ 
  end for
end for

```

Also for this tour, there are $\frac{n(n-1)}{2}$ configurations available. The advantage of the PCA tour (in comparison to the scatterplot tour) is that multivariate relations can be visually explored and semantics of the data are intrinsically emphasized, i.e., they cannot be missed.

3.6.3 Grand Tour

An orthography-preserving grand tour is an obvious extension of Asimov's grand tour [1]. Assuming a sampling in the space of orthographic configurations, the orthographic tour is given by connecting the samples with morphings. Orthographic grand tours share the same advantages and limitations of normal grand tours, namely the exponential complexity with n . Note that both PCA and orthographic grand tour reveal multivariate relations, but the grand tour is independent of the data. Clearly, the orthographic grand tour as well as the original grand tour [1] are only appropriate for low-dimensional data.

4 APPLICATIONS AND EVALUATION

As proof of concept, our approaches are subsequently evaluated. Please zoom into the figures on demand in order to recognize relevant and important details and information as well. For the evaluation, we sample nD spheres to generate synthetic data. With them, our concepts are illustrated w.r.t. distortion and orthography properties. Afterwards, several real data are applied to our techniques in order to clarify the advantages and to complete this discussion.

A point $\mathbf{m} = (m_1, m_2, \dots, m_n)^T$ that lies on the periphery of an nD sphere with radius r is given by

$$m_1 = r \cdot \cos(\phi_1), m_n = r \cdot \left(\prod_{j=1}^{n-1} \sin(\phi_j) \right), \\ m_i = r \cdot \left(\prod_{j=1}^{i-1} \sin(\phi_j) \right) \cdot \cos(\phi_i),$$

with $i = 2, \dots, n-1$. A dense random sampling of angles ϕ_j reveals our synthetic data.

In Fig. 12, our interaction approaches are evaluated w.r.t. a 5D sphere with 1500 samples and a radius of 0.2. From top to bottom, the following information are illustrated: Initialization and free movement interaction of an axis for traditional star coordinates and for RadViz. Distortions can be seen. Next: the evaluation of our analytical interaction approach. The same interaction is now implemented distortion-free (middle-right). However, a radial movement of the axis (black arrow, middle-left) gives the orthographic energy diagram on the right: the orthographic energy increases with growing interaction time (but slower than, e.g., for RadViz). This is a numerical effect of instability caused by enduringly solving a linear system (cf. Section 3.3.1), i.e., small errors add up over time. Afterwards, the evaluation of the two remaining interaction techniques is given: reconditioning and energy minimization ($\mu = 0.1, s = 5$); furthermore, their related orthographic energy diagrams can be seen. Both techniques preserve the orthographic property well, but the reconditioning works better with a magnitude of $25 \cdot 10^{-31}$ in comparison to $12 \cdot 10^{-4}$. In contrast, reconditioning gives an average drift of $d = 4 \cdot 10^{-5}$ (in our experiments) w.r.t. the goal axis \mathbf{p}_1^b , which limited its practicability. Thus, energy minimization should be preferred if such a drift is not acceptable. Below, our conditional orthography-preserving interaction approaches are investigated: the orthographic energy diagrams (right) show that the reconditioning ($s = 8$) preserves the orthography property much

better than the energy minimization ($\mu = 0.1, s = 5, g = 0.75$). Especially the use of fix conditions strongly influences this. That result has an easy explanation: the reconditioning enforces to preserve the orthography property. In comparison, the energy minimization does not, but it “blends” between the conditions and the orthographic property (steered by parameter g). In our experiments, the reconditioning minimizes – on average – the condition goal function f for each turn from $f_{start} = 0.0015$ to a minimum $f_{min} = 1.17 \cdot 10^{-4}$ (cf. Section 3.4), which illustrates that the reconditioning should be used in practice w.r.t. conditional interactions. Our interaction tools are also suitable for a larger number of dimensions, as illustrated in Fig. 13 (top, left to right) for $n = 50$.

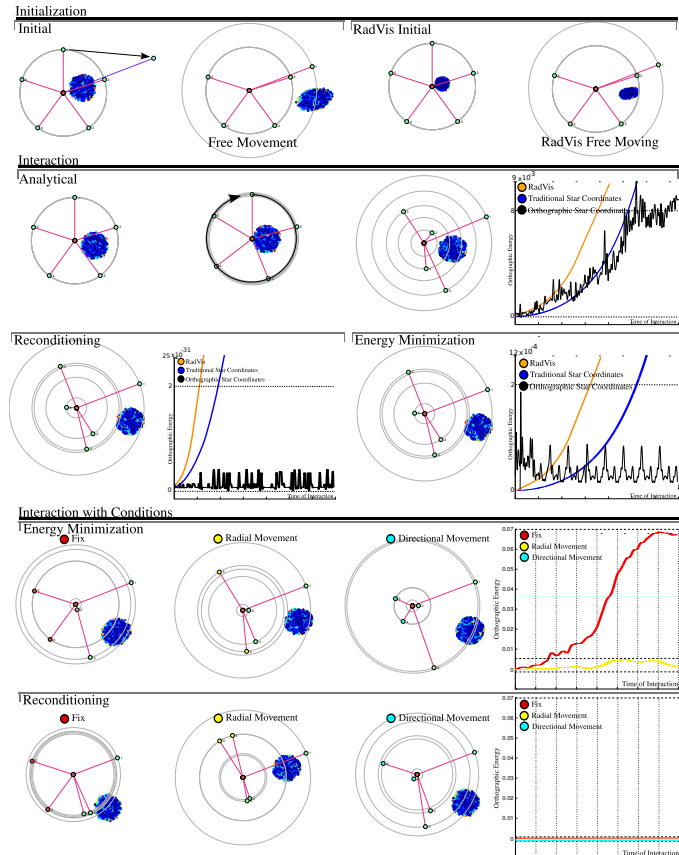


Fig. 12. Evaluations as well as comparisons for orthographic-preserving and classic interaction techniques, both illustrated for the case of $n = 5$.

Fig. 13 (bottom) and Fig. 14 illustrate the non-linearity of the orthography-preserving morphing concepts. In Fig. 13 (bottom) two scatterplots (left, middle-left) are given for the case $n = 5$. Fig. 13 (bottom; middle-right, right) shows the morphing – in a way that each step is plotted onto the previous one – for a simple blending and an orthography-preserved blending: It can be seen that the second approach preserves the orthography property for all intermediate steps, the simple blending does not. Fig. 14 also illustrates similar morphings for $n = 10, 20$, and 30 . It can be figured out that (i) a morphing is a non-linear operation and (ii) our approach implements this operation appropriately.

Fig. 15 shows a series of comparisons between RadViz, traditional star coordinates, and our orthographic star coordinates in several situations w.r.t. our interaction and morphing concepts. Note that all images are based on the same data configuration, namely three n D spheres with radius 0.2 and 1500 samples in each case, simulating in total 4500 data points. It can be seen that RadViz and traditional star coordinates neither preserve the size nor the shape, but orthographic star coordinates do. Fig. 16 shows a case study for the visual data exploration with orthographic star coordinates, for Iris data (4 di-

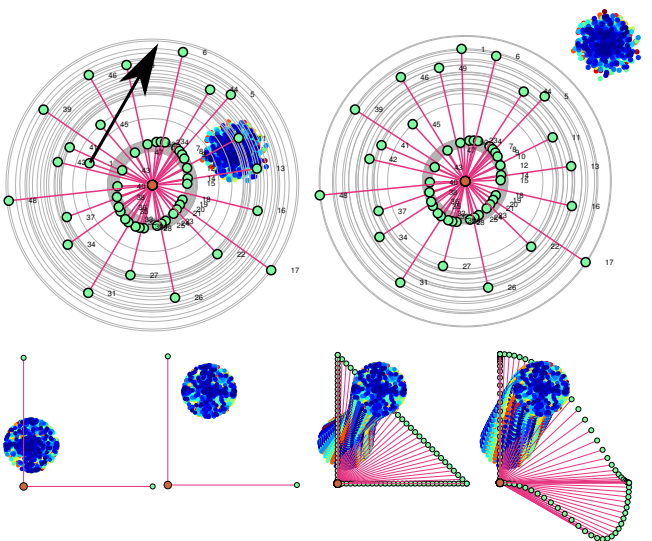


Fig. 13. Interaction and morphing: (top) orthographic interaction for $n = 50$, (down) orthographic morphing compared with simple blending.

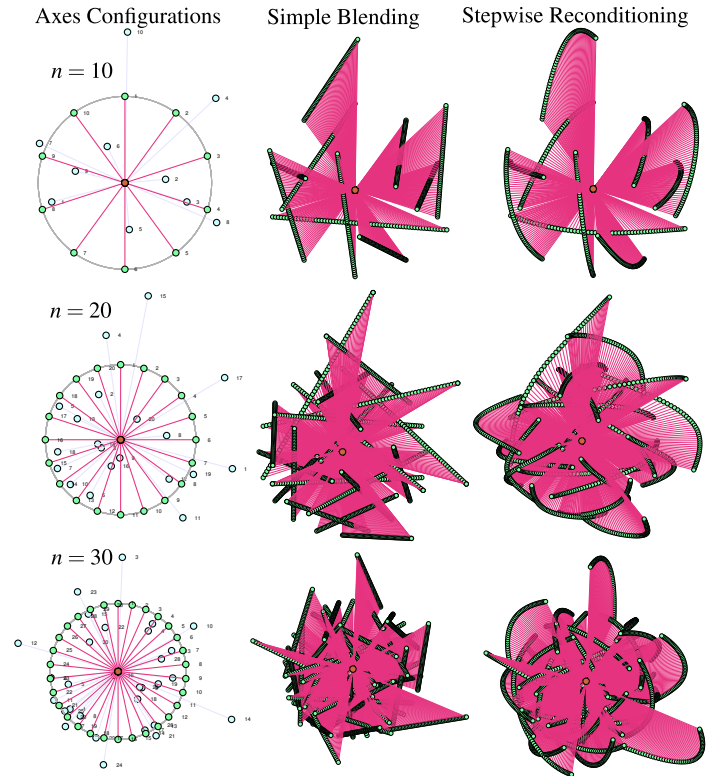


Fig. 14. Morphing: mutually compared for $n = 10, 20$, and 30 dimensions.

mensions, 150 records), Wine data (14 dimensions, 178 records), and Parkinson data (24 dimensions, 195 records). See [2] for details of the data. Please note that class information are not considered. Thus, each record has an individual color. For this figure, screenshots were captured while interacting with OSCs: from left to right and from top to bottom the interaction times grows. It can be seen that structures of the data turn out and a kind of rotation is observable. This is caused by the fact that an interaction with an OSC is exactly the following: a rotation of a high-dimensional hyperplane.

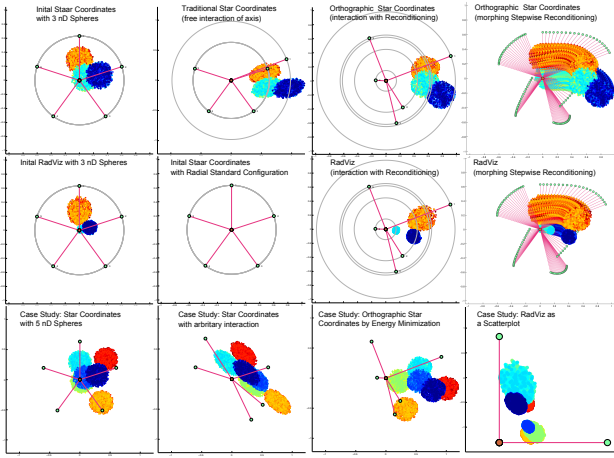


Fig. 15. Comparison of the visualization techniques RadViz, traditional star coordinates, and orthographic star coordinates for $n = 5$.

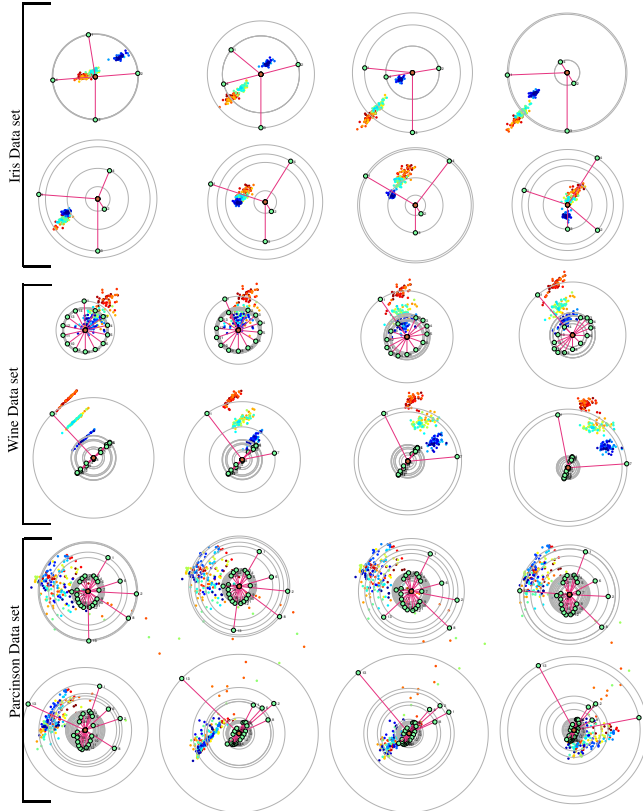


Fig. 16. Studies of visual data exploration by orthographic star coordinates for (top) Iris data set, (middle) Wine data set, and (down) Parkinson data set.

5 DISCUSSION

Low-dimensional projections are an appropriate approach to analyze high-dimensional data, but there are important differences to consider: both projective and affine projections cause distorted visualizations, as known from, e.g., RadViz (projective) and classical star coordinates (affine). By means of those distortions, local data properties might be focused as kind of a visual data lens, i.e., a certain sub-space of the data space is emphasized by this kind of data space lens. This allows a detailed local data space investigation and moreover an efficient use of the available screen space. On the other hand, these distortions might lead to wrong conclusions in terms of global patterns of the data and data space, respectively, since distortions visually hide, distort,

and interfere global patterns. In other words, non-orthographic projections do not allow a direct interpretation of the shape of n D spheres or patterns in general. Therefore, in order to facilitate a reliable investigation of global patterns, we introduced orthography-preserving multivariate projection as orthographic star coordinates. These orthographic projections complement projective and affine projections and they provide a distortion-free visual investigation of global patterns in the data space. The interplay of distortion-free and distorted low-dimensional multivariate projections facilitates a complete and complementary visual search of high-dimensional data in terms of local and global patterns within an iterative visual search process.

6 CONCLUSION

In this work, we propose an orthographic version of the popular star coordinates, as well as related interaction and morphing techniques. We extend our concepts to data tour approaches in order to reasonably visually reveal interesting patterns in the data. Our results show that orthographic star coordinates are convenient to avoid distortions and therefore to further improve the visual data exploration. Future work encompasses the discussion of 3D orthographic star coordinates.

APPENDIX

This appendix illustrates a scheme to reveal a linear system for the analytical orthography-preserving axis interaction w.r.t. certain dimension numbers n . See Fig. 6, the new axes are given by $\mathbf{p}_i^b = \mathbf{p}_i + \mathbf{s}_i; i = 1, \dots, n$ with $\mathbf{p}_i = (x_i \ y_i)^T, \mathbf{p}_i^b = (x_i^b \ y_i^b)^T, \mathbf{s}_i = (u_i \ v_i)^T, \mathbf{u} = (u_1, u_2, \dots, u_n)$, and $\mathbf{v} = (v_1, v_2, \dots, v_n)$. $\mathbf{s}_1 = (u_1 \ v_1)^T$ is given by the user, the remaining vectors $\mathbf{s}_i, i = 2, \dots, n$ can be calculated in order to preserve the orthographic property. For this, we derive three energy terms from Eq. (3-4) at first:

$$\begin{aligned} e_u(\alpha) &= \|\mathbf{x} + \alpha \cdot \mathbf{u}\|^2 - 1, \quad e_v(\alpha) = \|\mathbf{y} + \alpha \cdot \mathbf{v}\|^2 - 1, \\ e_{uv}(\alpha) &= -\mathbf{x} \cdot \mathbf{u} - \mathbf{y} \cdot \mathbf{v}. \end{aligned} \quad (8)$$

For an OSC, energy $e = 0$, i.e., the partial derivatives from (8) turn to zero: $\partial e_u(0)/\partial \alpha = \partial e_v(0)/\partial \alpha = \partial e_{uv}(0)/\partial \alpha = 0$. With this, a closed solution can be calculated for the unknowns u_2, u_3, v_2 as:

$$\begin{aligned} \begin{pmatrix} u_2 \\ u_3 \\ v_2 \end{pmatrix} &= \mathbf{U} \cdot \begin{pmatrix} b_1 = -2x_1u_1 + \sum_{i=4}^n -2x_iu_i \\ b_2 = -2y_1v_1 + \sum_{i=3}^n -2y_iv_i \\ b_3 = -u_1y_1 - v_1x_1 - v_3x_3 + \sum_{i=4}^n -u_iy_i - v_ix_i \end{pmatrix}, \text{ with} \\ \mathbf{U} &= \begin{pmatrix} a_{11} = \frac{0.5y_3}{x_2y_3 - x_3y_2} & a_{12} = \frac{0.5x_3x_2}{y_2(x_2y_3 - x_3y_2)} & a_{13} = \frac{-x_3}{x_2y_3 - x_3y_2} \\ a_{21} = \frac{-0.5y_2}{x_2y_3 - x_3y_2} & a_{22} = \frac{-0.5x_2^2}{y_2(x_2y_3 - x_3y_2)} & a_{23} = \frac{x_2}{x_2y_3 - x_3y_2} \\ 0 & a_{32} = \frac{1}{2y_2} & 0 \end{pmatrix}. \end{aligned}$$

In addition, the squared Euclidean distance h for \mathbf{u} and \mathbf{v} is given by

$$h = \sum_{i=2}^n u_i^2 + v_i^2 = [u_2^2 + u_3^2 + v_2^2] + \left[\sum_{i=4}^n u_i^2 + \sum_{i=3}^n v_i^2 \right]$$

By considering the known variables u_2, u_3 and v_2 , this yields:

$$h = \left[\left\| \mathbf{U} \cdot (b_1 \ b_2 \ b_3)^T \right\|^2 \right] + \left[\sum_{i=4}^n u_i^2 + \sum_{i=3}^n v_i^2 \right]$$

We urge to minimize h to get the remaining unknowns, i.e., the partial derivatives $\frac{\partial h}{\partial u_i} = \frac{\partial h}{\partial v_i} = 0$ vanish. By use of a formula manipulation system like Maple, a closed form of the partial derivatives follows:

$$\frac{\partial h}{\partial u_i} = 2(u_2(-2a_{11}x_i - a_{13}y_i) + u_3(-2a_{21}x_i - a_{23}y_i) + u_i),$$

$$\frac{\partial h}{\partial v_i} = 2(u_2(-2a_{12}y_i - a_{13}x_i) + u_3(-2a_{22}y_i - a_{23}x_i) + v_i - 4v_2a_{32}^2y_i).$$

The unknowns and knowns are now linearly related, i.e., solving the linear system $(\frac{\partial h}{\partial u_i} \ \frac{\partial h}{\partial v_i})^T = \mathbf{0}$ yields shift vectors in \mathbf{u} and \mathbf{v} that guarantee an orthographic projection after interaction with $\mathbf{s}_1 = (u_1 \ v_1)^T$.

REFERENCES

- [1] D. Asimov. The Grand Tour: a Tool for Viewing Multidimensional Data. *Journal on Scientific and Statistical Computing*, 6(1):128–143, 1985.
- [2] A. Asuncion and D. J. Newman. UCI Machine Learning Repository. University of California, Information and Computer Sciences, 2007.
- [3] A. Bordignon, R. Castro, H. Lopes, T. Lewiner, and G. Tavares. Exploratory Visualization based on Multidimensional Transfer Functions and Star Coordinates. In *XIX Brazilian Symposium on Computer Graphics and Image Processing*, pages 273 – 280, 2006.
- [4] D. Cook, A. Buja, J. Cabréa, and C. Hurley. Grand Tour and Projection Pursuit. *Journal of Computational and Statistical Computing*, 4(3):155 – 172, 1995.
- [5] K. M. Daniels, G. G. Grinstein, A. Russell, and M. Glidden. Properties of Normalized Radial Visualizations. *Information Visualization*, 11(4):273–300, 2012.
- [6] L. Di Caro, V. Frias-Martinez, and E. Frias-Martinez. Analyzing the Role of Dimension Arrangement for Data Visualization in RadViz. In *Proceedings of the 14th Pacific-Asia conference on Advances in Knowledge Discovery and Data Mining - Volume Part II*, pages 125–132, 2010.
- [7] R. O. Duda, P. E. Hart, and D. G. Stork. *Pattern Classification (2nd Edition)*. Wiley-Interscience, 2000.
- [8] G. Farin. *Curves and Surfaces for CAGD: a Practical Guide*. Morgan Kaufmann Publishers Inc., 5th edition, 2002.
- [9] D. Freedman. *Statistical Models: Theory and Practice*. Cambridge University Press, 2005.
- [10] J. H. Friedman. Exploratory Projection Pursuit. *Journal of the American Statistical Association*, 82(397):249 – 266, 1987.
- [11] J. H. Friedman and J. W. Tukey. A Projection Pursuit Algorithm for Exploratory Data Analysis. *IEEE Transactions on Computers*, 23:881–890, 1974.
- [12] M. Friendly. *SAS System for Statistical Graphics*. SAS Publishing, 1st edition, 1991.
- [13] P. Hoffman, G. Grinstein, K. Marx, I. Grosse, and E. Stanley. Dna Visual and Analytic Data Mining. In *Proceedings of the 8th Conference on Visualization*, pages 437–ff., 1997.
- [14] P. Hoffman, G. Grinstein, and D. Pinkney. Dimensional Anchors: a Graphic Primitive for Multidimensional Multivariate Information Visualizations. In *Workshop on New Paradigms in Information Visualization and Manipulation*, pages 9–16, 1999.
- [15] H. Hotelling. Analysis of a Complex of Statistical Variables into Principal Components. *Journal of Educational Psychology*, 24(6):417 – 441, 1933.
- [16] J. M. Chambers, W. S. Cleveland, B. Kleiner, and P. A. Tukey. *Graphical Methods for Data Analysis*. Chapman and Hall, New York, 1983.
- [17] I. Jolliffe. *Principal Component Analysis*. Springer Verlag, 1986.
- [18] E. Kandogan. Star Coordinates: A Multi-Dimensional Visualization Technique with Uniform Treatment of Dimensions. In *Proceedings of the IEEE Information Visualization Symposium*, pages 9–12, 2000.
- [19] E. Kandogan. Visualizing Multi-Dimensional Clusters, Trends, and Outliers Using Star Coordinates. In *Proceedings of the seventh ACM SIGKDD international Conference on Knowledge Discovery and Data Mining*, pages 107 – 116, 2001.
- [20] L. N. Trefethen and D. Bau III. *Numerical Linear Algebra*. Society for Industrial and Applied Mathematics, 1997.
- [21] K.-L. Ma and S. T. Teoh. StarClass: Interactive Visual Classification Using Star Coordinates. In *Proceedings of the 3rd SIAM International Conference on Data Mining*, pages 178–185, 2003.
- [22] V. Molchanov, A. Fofonov, and L. Linsen. Continuous Representation of Projected Attribute Spaces of Multifields over Any Spatial Sampling. In *Computer Graphics Forum (Proceedings of Eurovis)*, 2013.
- [23] L. Nováková. *Visualization Data for Data Mining*. PhD thesis, Czech Technical University in Prague Faculty of Electrical Engineering, Department of Cybernetics, Prague, Czech, 2009.
- [24] L. Nováková and O. Štepánková. Multidimensional Clusters in RadViz. In *Proceedings of the 6th WSEAS International Conference on Simulation, Modelling and Optimization*, pages 470–475, 2006.
- [25] L. Nováková and O. Štepánková. Visualization of Trends Using RadViz. *Journal of Intelligent Information Systems*, 37(3):355–369, 2011.
- [26] J. Shaik and M. Yesin. Visualization of High Dimensional Data Using an Automated 3D Star Co-ordinate System. *IEEE International Joint Conference on Neural Networks*, pages 2318–2325, 2006.
- [27] H. Theisel and M. Kreuseler. An Enhanced Spring Model for Information Visualization. *Computer Graphics Forum (Proceedings of Eurographics)*, 17(3):335–344, 1998.